Rotorcraft Downwash Flow Field Study to Understand the Aerodynamics of Helicopter Brownout

Alan J. Wadcock
NASA Ames Research Center
Alan.J.Wadcock@nasa.gov

Lindsay A. Ewing
NASA Ames Education Associates Program
lewing@mail.arc.nasa.gov

Eduardo Solis
Monterey Technologies, Inc
esolis@mail.arc.nasa.gov

Mark Potsdam
US Army Aeroflightdynamics Directorate
mpotsdam@mail.arc.nasa.gov

Ganesh Rajagopalan
Iowa State University
nappi@sukra-helitek.com

Abstract

Rotorcraft brownout is caused by the entrainment of dust and sand particles in helicopter downwash, resulting in reduced pilot visibility during low, slow flight and landing. Recently, brownout has become a high-priority problem for military operations because of the risk to both pilot and equipment. Mitigation of this problem has focused on flight controls and landing maneuvers, but current knowledge and experimental data describing the aerodynamic contribution to brownout are limited. This paper focuses on downwash characteristics of a UH-60 Blackhawk as they pertain to particle entrainment and brownout. Results of a full-scale tuft test are presented and used to validate a high-fidelity Navier-Stokes computational fluid dynamics (CFD) calculation. CFD analysis for an EH-101 Merlin helicopter is also presented, and its flow field characteristics are compared with those of the UH-60.

Notation

C_T = thrust coefficient
IGE = in ground effect
OGE = out of ground effect
r = radial distance
R = rotor radius
Ψ = azimuthal location

Introduction

Rotorcraft brownout is a critical problem experienced by helicopters when landing in dry, sandy ground conditions. (Helicopters landing in powdery snow experience a similar problem referred to as whiteout). Brownout is caused by dust particles that get entrained in the rotor downwash while the helicopter is in ground effect. The dust can reduce or completely obscure the pilot's visibility of the ground and horizon, which are two important orientation cues used for landing (Figure 1). Due to recent military activity in desert environments, brownout has become a high priority problem for helicopter pilots. Many pilots consider landing in dust to be the most difficult and dangerous maneuver in Army aviation [1]. Furthermore, extended operations in brownout can lead to damage of engine components and rotor blades. The U.S. Army spends approximately $100 million per year on maintenance problems and equipment loss related to brownout, and reports that brownout is responsible for 3 out of every 4 accidents in Iraq and Afghanistan [2]. Brownout compromises the safety of pilots, crew and equipment, and accounts for a significant number of military accidents and the loss of valuable resources.

Current research efforts to help mitigate brownout include the development of flight control systems, landing maneuvers, prepared landing pads and sensors that can see through the airborne dust [3]. To assist in the development of these techniques and devices, an understanding of the physics of brownout is desirable. This includes quantifying the characteristics of the ground vortex in the helicopter wake, the entrainment of sand particles, and the resulting obscuration.

Due to a large variance in helicopter design, quantifying the ground vortex is a difficult task. Factors such as disk loading, number of blades, blade radius, blade root cutout, blade chord, blade twist,

Presented at the American Helicopter Society Southwest Region Technical Specialists' Meeting, "Technologies for the Next Generation of Vertical Lift Aircraft," Dallas-Fort Worth, TX, October 15-17, 2008.

rotor RPM, blade geometry, tip vortex strength and dynamics, rotor orientation and configuration, ground proximity, and fuselage configuration (fuselage shape and window locations) may all have an effect on helicopter (or pilot) performance under brownout conditions [4]. Conventional wisdom dictates that rotorcraft with low disk loading perform better in brownout because they produce lower outwash velocities than rotorcraft with high disk loading. However, Table 1 shows that the AgustaWestland EH-101 Merlin (a helicopter that is advertised as creating a curtain of clear air, pushing sand and debris away from the aircraft in brownout conditions) actually has a higher disk loading than the Sikorsky HH-60G Blackhawk, a helicopter that suffers from severe brownout. AgustaWestland claims that the EH-101 ring of clear air, referred to as the "donut effect", is due to its BERP (British Experimental Rotor Programme) advanced blade tip design (Figure 2). However, a similar blade tip is used on the Lynx helicopter, and apparently has no effect on reducing the severity of brownout for this helicopter. Fuselage size and blade root cutout have also been suggested as contributing to brownout performance. Since no brownout test data for the EH-101 exists (in the public domain), it is not clear what factors produce the donut effect, and under what flight conditions the donut effect exists.

In order to understand how rotorcraft design characteristics affect brownout, more information about helicopter downwash in ground effect is required. Previous work has been done to computationally model helicopter downwash both in and out of ground effect and to simulate brownout [6-10], but little experimental data exists for code validation. At NASA Ames Research Center, a full-scale flight test was recently performed to study the outwash from a UH-60L Blackhawk, an OH-58C Kiowa, an MD-500, and an unmanned autonomous Yamaha RMAX. Each rotorcraft airframe was tufted in the vicinity of the cabin and flown in hover over a grid of ground tufts. Video and high-resolution digital still photographs were taken to document the airflow on the airframe and on the ground plane under the rotor disk. Only data from the UH-60L will be discussed in the current paper. The focus of this paper is to present results from this full-scale flight test of the UH-60L as well as results from CFD analyses for a UH-60 and an EH-101. Flight test and CFD results for the UH-60 will be compared and contrasted with CFD results for the EH-101.

Particle Entrainment

Brownout can be divided into three separate processes that need to be understood: helicopter downwash, particle entrainment, and visual obscuration. This paper focuses on understanding helicopter downwash velocity fields, but an understanding of particle entrainment is also necessary to determine how the rotor downwash interacts with individual particles.

Bagnold [11] defines the three main transport modes for sand to be surface creep, saltation and suspension (Figure 3). Surface creep occurs for low-speed flows where the fluid only exerts enough force on the sand particle for it to roll along the surface of the bed. Higher wind velocities result in saltation. During saltation a particle is initially lifted off the ground by collisions with other particles and by larger aerodynamic forces associated with the higher wind velocities. As the particle moves away from the ground and into the airstream, its velocity relative to the wind decreases, producing less lift. When the particle weight becomes greater than the lift force acting on it, the particle sinks back toward the ground in a parabolic trajectory. When the particle impacts the ground, the saltation process is repeated. Suspension occurs when the particle is transported upward by turbulent eddies and carried along in the airstream. For a given particle size, there is a critical wind velocity at which the particle is able to transition from saltation to suspension. During this transition, the process of how particles are ejected from the bed changes from being determined by impact collisions to being determined primarily by aerodynamic lift forces [13].

Experimental Study of Full-Scale UH-60L in Hover

Recently, the U. S. Army has experienced a large loss of aircraft in Afghanistan and Iraq due to brownout accidents (at one time 3 out of 4 aircraft accidents), and the single largest cause of UH-60 attrition is brownout. For this reason DARPA initiated the Sandblaster Program at Yuma Proving Grounds, where several helicopters were flown under controlled brownout conditions. DARPA was researching sensors that could see through the airborne dust cloud and use "aircraft memory" by recording the landing area and factoring in the aircraft motion immediately prior to brownout to assist the pilot in landing the aircraft once pilot visibility became lost. In addition, suggested flight controls for the future were to enable the aircraft to

hold hover position, hold hover attitude, and "beep down" where the pilot has a button which would incrementally lower the aircraft in hover a set amount each beep. One area that was absent from the investigation was the effect of aerodynamic design.

The U. S. Army flies two UH-60 aircraft out of NASA Ames Research Center. The availability and immediate proximity of these aircraft presented NASA the opportunity to document the flow field of the UH-60 while flying under brownout conditions, without actually having the aircraft fly over dusty or sandy ground. The goal was to obtain as much data about the flow field as possible, and to understand what features of the UH-60 make the aircraft susceptible to brownout.

One of the first tests performed on the UH-60 was an attempt to visualize the ground vortex shape and location with respect to the aircraft, as a function of wheel height above ground and aircraft speed. For flight tests inside the confines of Moffett Field, approval was readily granted to fly above the median strip on either side of the main runways. These areas are wasteland where only weeds grow. At midsummer, the weeds were 1-ft tall or higher, but brown, dry, and sparse. In addition to coordination with the control tower, these flights required two pilots for the UH-60 and a third pilot plus photographer for the chase aircraft. Both Sony HD730 camcorder video (recording in HDCAM format, 1440 x 1080 pixels) and Nikon D200 SLR digital stills (4288 x 2848 pixels) were acquired. Unfortunately, little useful information was garnered. The ground vortex was barely visible on the HD video recording, and the high-resolution still photographs were completely undecipherable. If a grassy meadow had been available the chance of success may have been greater, relying on the different reflectivity of grass leaves (standing up or blown flat) to delineate the ground vortex location.

Several other flow visualization techniques were considered including flight over water, smoke and neutrally buoyant soap bubbles. Unfortunately, flight over salt water was denied due to corrosion risk and flight over fresh water was deemed not feasible because it required obtaining permission for off-base flight from outside agencies. Permission to use either smoke or soap bubbles was denied because those materials could also lead to possible corrosion of the aircraft.

Ultimately, research goals were reconsidered and the decision was made to concentrate efforts on *hover* flow field measurements in an attempt to reveal hover characteristics of the UH-60 that could influence brownout performance.

A 60 ft x 60 ft grid of 1-ft long tufts, each placed 1 ft apart, was created on the flight line ramp. The total number of ground tufts was 60 x 61 = 3660. Ground plane tufts made from black 4-ply yarn were secured to the ground with a quarter size amount of white silicone adhesive. Helicopter fuselage tufts were chosen according to airframe size and predicted downwash velocities to ensure that they would effectively show the instantaneous flow direction on the airframe. Color of tuft was chosen to provide maximum contrast with airframe color. The UH-60 airframe tufts were white, 4-ply acrylic yarn secured by 200 mph green tunnel tape. Each tuft was 6.5 inches long, positioned in columns spaced 6 inches apart horizontally. No tufts were placed on the windows or near the engine intake at the pilot's request. The UH-60L was tufted on the port side of the airframe from the nose of the aircraft to slightly downstream of the rotor hub. Interest was concentrated in the vicinity of the cockpit to determine if the flow was directed either up or down adjacent to the pilot seat, and at the hub to show how large an effect the root cutout plays in allowing upwards flow through the rotor disk adjacent to the rotor hub.

The UH-60 was flown in hover above the tuft grid at wheel heights of 5 ft, 10 ft, 20 ft, 30 ft, 40 ft, and 50 ft. Wheel heights quoted in this paper refer to nominal wheel heights estimated by individual pilots. No direct measurements of wheel height or rotor height were made.

All tuft studies were performed in the early morning, generally between 7:30am and 9:30am, to take advantage of low wind conditions. Winds were always less than 3 knots, and by themselves were insufficient to move the ground plane tufts. Only the operation of the rotor above the ground plane tuft grid was sufficient to move the ground plane tufts. In the early morning, before the sun had moved significantly above the horizon, a marine layer several hundred feet thick was generally found to exist about a hundred feet above the ground. This was ideal for tuft photography, as the diffuse light from the sun did not cast a shadow from the fuselage on the ground plane tuft grid. Later in the day, when the marine layer had burned off and the sun had risen higher in the sky, the airframe shadow was found to obscure the black tufts against the dark concrete background.

Each pilot used bright orange plastic cones as alignment aides. A pair of cones was aligned ahead of the grid and a single cone placed outside the grid on each side of the rotor hub, sufficiently far from the rotor for the pilot to see all 4 cones.

At each aircraft height, HD video (1440 x 1080 pixels) and high-resolution digital still images (4288 x 2848 pixels) of the ground tufts were taken from an adjacent three-story roof near the flight line. Still images of the airframe tufts were also taken from ground level on the port side of the aircraft.

The tuft study on the UH-60L proved to be so successful that the hover program was immediately expanded to include additional aircraft: the OH-58, the MD-500, and the Yamaha RMAX autonomous helicopter. All these aircraft were studied both in and out of ground effect and were chosen because they were readily available at NASA Ames. Only data from the UH-60L will be discussed in the current paper.

Results and Discussion of Tuft Study on UH-60L in Hover

Figures 4(a) through 4(c) show single instantaneous photographs of airframe tufts on the UH-60L hovering out of ground effect (OGE) at 50-ft wheel height. Figure 4(d) represents an overlay of all 3 instantaneous images, providing information on average tuft direction and degree of flow steadiness (from degree of tuft coning) at this wheel height. The flow is clearly not steady. However, in general, tufts are seen to be pointing downwards on the side of the airframe (in the direction of the rotor downwash) indicating attached flow.

Figures 5(a) through 5(c) show single instantaneous photographs of airframe tufts on the UH-60L hovering in ground effect (IGE) at 5-ft wheel height. Many tufts can be seen pointing upwards toward the rotor and away from the ground. Figure 5(d) represents an overlay of all 3 instantaneous images providing information on average tuft direction and degree of steadiness. In general, for the rotor in ground effect, the airframe tufts are very unsteady (the degree of unsteadiness increasing as the rotor approaches the ground). Many tufts show a large range of motion including complete reversal of flow direction. In general, tufts near the rotor hub tend to be pointing upwards.

Of particular interest is the case of the UH-60L with wheels on the ground, since this minimizes any flow unsteadiness due to pilot induced motions of the rotor. Ground plane tuft images were acquired with the UH-60L with wheels on the ground, rotor spinning at full rpm with collective at 75% of hover value. Figure 6 shows a single instantaneous photograph of the UH-60L with wheels on the ground, the image being taken from the roof of an adjacent building. All photographs of the ground plane tufts were acquired from this vantage point as described earlier. The original oblique view of the ground plane tufts shown in Figure 6 is difficult to interpret. Using Adobe Photoshop™, this image has been reoriented to show the ground plane tufts from a birds-eye view. Figure 7 shows Figure 6 after reorientation. This represents the view an observer would see from immediately above the center of the tuft grid. Because the image has been reoriented, the airframe shown in the upper right hand corner of Figure 7 appears warped. One feature in Figure 7 that should be readily recognized from Figure 6 is the white boom protruding from the front of the aircraft. The rotor disk and an outline of the airframe in plan view have been added for clarity. To remove the 180-degree directional ambiguity associated with any tuft, note that the silicone adhesive used to anchor the tuft to the ground is white. The instantaneous flow pattern under the rotor disk appears relatively disorganized. Figure 8 shows the result of averaging 25 such instantaneous images acquired every 3-seconds over a period of 1 minute and 15 seconds. Significant tuft coning is an indication of flow unsteadiness in Figure 8. Minimal tuft coning is an indication of steady flow. No tuft coning is an indication that the tuft has become entangled with an adjacent tuft or has become stuck to the ground.

Figure 9 represents an instantaneous ground-plane tuft pattern for the UH-60L at 20-ft wheel height above ground. Once again, the UH-60L airframe outline and the rotor disk have been added in plan view to simplify interpretation. Flow direction appears somewhat random until the tuft pattern is studied carefully. Examination of the tuft pattern outside the rotor disk shows that the flow direction is typically close to radially outwards, as expected. Under the inner part of the rotor disk, on either side of the fuselage, the tufts clearly indicate flow radially *inwards* towards the rotor hub. Approximately 13.5ft either side of the fuselage there exist stagnation lines where the lateral velocity component is close to zero (y/R = 50% +/-4%). For clarity, a pair of white lines has been added to Figure 9 to identify the locations of the stagnation lines described above.

Figure 10 represents the average of 100 such instantaneous tuft images acquired every 3-seconds

over a period of 5 minutes. Figure 10 provides an average location for the stagnation lines at approximately y/R = 56%+/-4%.

Figures 4 through 10 provide useful information regarding instantaneous or mean flow direction on the airframe or on the ground plane directly beneath the rotor disk. However, information about the flow away from the airframe and ground surfaces is lacking. These figures do not provide information on velocity components (or even flow direction) in the vicinity of the hub where upwash through the rotor disk might be expected (both IGE and OGE). The location of stagnation streamlines on the ground plane either side of the fuselage have been identified, but streamlines starting in the rotor disk and ending at these stagnation lines on the ground plane are undefined. This information is important, since only flow *outside* of this radial location in the rotor plane will contribute to outwash. This is where CFD can prove useful by providing the full three-dimensional solution.

CFD Model of UH-60

The results of a *turbulent* Navier-Stokes computation designed to model a UH-60 helicopter hovering in ground effect at a wheel height of 20 ft (corresponding to a rotor disk about 0.6 diameters above the ground) are presented in Figures 11 through 15. These results were obtained using the code OVERFLOW 2 [14, 15] with the Spalart-Allmaras turbulence model. Both the UH-60 fuselage and simplified hub were modeled. The main rotor was modeled as an actuator disk. The quasi-steady actuator disk model does not provide for generation of discrete tip vortices although swirl is modeled. The momentum source strength was defined by blade element theory with UH-60 defined rotor characteristics (UH-60 airfoils, twist distribution, RPM and tail rotor thrust). No tip loss model was used. The tail rotor was modeled as a uniform pressure disk (no swirl). The fuselage was modeled at a 3-degree nose-up attitude so that the rotor was parallel to the ground. The rotor was trimmed for thrust only (not moments or flapping). The target C_T was 0.0065. The total solution duration was 15 equivalent rotor revolutions following a solution that was run to "steady state" in order to initialize the flow field. The mean flow field is the result of averaging the solution over the final 9 equivalent rotor revolutions.

Figure 11 shows the CFD grid. Figure 12 shows the computed *mean* velocity vectors in the centerline plane from the UH-60 CFD analysis. Note the recirculation through the rotor disk close to the rotor hub, as suspected from the full-scale tuft study of the UH-60L airframe. Upwash through the rotor disk is predicted for the innermost 21% of the blade radius. Compare this to the root cutout value of 19% shown in Figure 11. The highest downwash velocities are observed at the rotor tip.

Figure 13 shows computed *mean* velocity components in the transverse plane through the rotor hub. Once again, recirculation through the rotor disk is evident close to the rotor hub. At azimuth 90 degrees and 270 degrees, the upwash through the rotor disk is shown to extend over 25% of the blade radius and upwash is evident along both sides of the airframe (also confirmed by airframe tuft photographs). The expected initial wake contraction is evident immediately below the rotor disk and very weak recirculation is evident beneath the fuselage. The ground plane radial velocity is shown to be zero close to r/R = 0.66 in this figure. This is further outboard than indicated by observations of ground plane tufts (see Figures 9 and 10) and the disagreement appears to be somewhat larger than experimental uncertainty would indicate. The CFD calculation predicts that the stagnation line on the port side of the airframe is slightly further from the aircraft hub than on the starboard side. This is confirmed by the mean tuft pattern shown in Figure 10.

Figure 14 shows the computed velocity components in a horizontal plane 1ft above the ground. Note the relatively low outwash velocity components parallel to the ground at all points under the rotor disk. Peak outwash velocity is reached a small distance *outside the rotor disk*. This is an important observation. Low shear may be expected beneath regions of low outwash velocity and high shear may be expected beneath regions of high outwash velocity. Shear stress controls saltation so particle entrainment is more likely outside the rotor disk than beneath the rotor disk. Considering that part of the ground plane flow field *outside the rotor disk*, there is a region of low outwash velocity in the range $150^o < \Psi < 240^o$, ahead of the airframe. This reduction in outwash velocity is presumably related to the airframe wake. The largest reduction in outwash velocity occurs in the vicinity of Ψ = 210 degrees, presumably due to the residual swirl in the rotor downwash. The maximum reduction in outwash velocity is modest --- perhaps 20% less than neighboring locations. There is a similar region of reduced outwash velocity at approximately Ψ = 30 degrees (behind the aircraft)

but this is of less importance because it is far behind the pilot and therefore out of view.

Figure 15 shows the result of overlaying the computed mean surface flow lines (shear stress vectors) on top of the average ground plane tuft pattern (from Figure 10). Red represents high shear and blue represents low shear. This image is particularly useful in revealing the stagnation lines on each side of the fuselage (Ψ = 90 and Ψ = 270 degrees) separated by a distance of about 66%+/-4% of the rotor diameter. Note that this computed distance is greater than the 56% of the rotor diameter seen in the full-scale UH-60L tuft study.

Strictly speaking, the magnitude of shear stress needs to be examined in order to determine where particles will become airborne. However, looking at Figure 14 (outwash velocities) and Figure 15 (ground plane shear stress), the peak values for both occur *outside the rotor disk*. This implies that particle entrainment most likely occurs *outside* the rotor disk. This is confirmed by observation of UH-60 take-offs from hardpan at Yuma Proving Grounds. The UH-60 generated no airborne material while sitting on the ground at minimum collective and full RPM. Upon pulling collective, a few small wisps of spinning sand (presumably related to the passage of tip vortices) were observed close to the ground under the edge of the rotor disk. A short distance outside the rotor disk the ground "exploded" as huge volumes of sand and dust became airborne ----- exactly where one would expect based on knowledge of peak outwash velocity. Directly beneath the rotor disk the air was free from sand and dust. Within a few seconds, the UH-60 was airborne and had climbed out of the enveloping dust cloud.

CFD Model of EH-101

The results of a *laminar* Navier-Stokes computation designed to model the EH-101 helicopter hovering in ground effect at a wheel height of 19.2 ft (corresponding to a rotor disk about 0.6 diameters above the ground) are presented in Figures 16 through 20. These results were obtained using the code ROT3DC [16-19]. Turbulent computations are an option when using this code, but for the current study laminar computations were performed in the interest of expediency. The flow is without question turbulent, but the laminar computation is expected to capture all salient features of the flow apart from the shear stress on the ground plane.

The main rotor was modeled as an actuator disk. Once again, the actuator disk model does not provide for generation of discrete tip vortices although swirl is modeled. Rotor blades drawn in Figures 16 through 20 are fictional --- the actuator disk model does not model individual blades. The momentum source strength was defined by blade element theory with EH-101 estimated rotor characteristics (61ft diameter main rotor, rotor speed of 210 rpm, 5 blades, -12 degree twist, a combination of XV-15 and CH-47 airfoils and BERP tip). The fuselage was modeled as a simplified 1986 EH-101 airframe. The airframe was modeled 3.8 degrees nose up to place the rotor disk parallel to the ground. Three cases were calculated for a C_T of 0.0100 and a rotor height of 36.6 ft above ground (0.6 rotor diameters above ground — IGE).

First, the isolated rotor with no root cutout was modeled. Figure 16 shows computed velocity vectors in the transverse plane through the rotor hub. The expected initial wake contraction is evident just below the rotor disk. Recirculation through the rotor disk is evident in the vicinity of the rotor hub. Upwash appears limited to r/R < 34%. This is a surprisingly large area of upwash through the rotor disk considering that there is no root cutout modeled. Flow through the rotor disk is seen to stagnate on the ground plane close to r/R = 90%. Large regions of recirculation are evident under the rotor disk.

Second, the isolated rotor was modeled with 16.4% root cut out. Figure 17 shows computed velocity vectors in the transverse plane through the rotor hub. The largest change from the prior flow field can be seen in the vicinity of the rotor hub, where very strong upwash through the rotor disk is now indicated. Upwash through the rotor disk is evident for r/R < 28% (smaller extent than without root cutout!). Twin recirculation regions under the rotor disk are evident with stagnation on the ground plane at r/R = 80%. Inclusion of the root cutout significantly increased the magnitude of the velocity upwash through the rotor disk at the hub and brought the stagnation points on the ground plane slightly closer together.

The third and final geometry analyzed was the complete rotor (with root cutout) and fuselage model, with computed velocity vectors as shown in Figures 18 through 20. Very little recirculation is observed near the rotor hub in Figure 18. What little upwash exists lies within r/R < 22%, so the fuselage has significantly reduced both the extent of upwash through the rotor disk and the magnitude of this upwash velocity. In Figure 18 the stagnation points on the ground plane occur at r/R = 73%, indicating

that the inclusion of the airframe brought the ground plane stagnation points even closer together. Note, however, that they are still quite far from the rotor hub. Well-organized recirculation regions are seen beneath the fuselage, but *upwash is not predicted on either side of the airframe*. The current study had no opportunity to study the full-scale vehicle using tufts, so there is no means of knowing if these calculations are borne out by observation. If this computation is correct, then the EH-101 airframe does not have upwash along each side of the cabin, unlike the UH-60. There is a small amount of asymmetry in the mean flow (side to side), as also observed in the UH-60 computations. The predicted ground plane stagnation points for the EH-101 are considerably further apart than observed for the UH-60L. The strong recirculation regions predicted beneath the fuselage of the EH-101 are absent from the UH-60 computations (Figure 13). Any energy extracted from the mean rotor downwash and dissipated beneath the fuselage leaves less energy available to appear in the rotor outwash.

Figure 20 shows computed velocity vectors in the horizontal plane 1ft above the ground. Note that peak rotor outwash occurs *outside* the rotor disk. Velocities are higher than for the UH-60 primarily due to the higher C_T used for the EH-101. Analysis of the Navier-Stokes computations for the UH-60 showed a strong correlation between the magnitude of the outwash velocity in the 1ft plane and the underlying shear stress at ground level. Applying this observation to the ROT3DC computed velocities in the 1ft plane allows for this velocity map to be interpreted as a shear stress map. Figure 20 shows reduced rotor outwash (and therefore reduced shear stress at the ground) for $170^o < \Psi < 220^o$ with the largest reduction in outwash velocity in the vicinity of Ψ=195 degrees, presumably due to the airframe wake and the residual swirl in the downwash (in the direction of blade rotation). The maximum reduction in outwash velocity is significant --- possibly 40% less than neighboring locations. A similar feature was observed in the Navier-Stokes computations for the UH-60 at a slightly different azimuthal location in front of the cabin (about Ψ=210 degrees in Figure 14). This means that if a region of reduced particle entrainment (and less severe brownout) exists due to the lower outwash velocities, it would be more in front of the pilot in the EH-101 than in the UH-60.

The EH-101 nose location is seen to be located unusually far forward under the rotor disk in Figure 20. Nose location is estimated to be at r/R = 70% ahead of the rotor hub. The bluff nature of the cabin nose for the EH-101 (Figure 19) is obvious in comparison to the streamlined nature of the UH-60 cabin nose (Figure 12). The airframe wake evidently plays a role in the outwash distribution at ground level. If the airframe nose is located unusually far forward (as is the case for the EH-101), it is not unreasonable to expect reduced outwash in the 3rd quadrant, reduced shear stress, reduced particle entrainment, and improved brownout visibility.

Summary

Tuft patterns were observed on the airframe of a full-scale UH-60L helicopter while hovering both in and out of ground effect. Instantaneous airframe tuft patterns are presented for a range of wheel heights above ground. Overlays of instantaneous tuft patterns are presented to provide an indication of flow steadiness. While out of ground effect, airframe tufts indicated attached flow with the tufts pointing towards the ground. As the helicopter altitude decreased and the rotor moved into ground effect, the flow became increasingly unsteady. With the rotor in ground effect, airframe tufts were shown to point upwards, towards the rotor.

The UH-60L was flown in hover above a tufted ground plane. Instantaneous and mean ground plane tuft patterns were presented for both zero and 5-ft wheel height above ground. Ground plane tuft patterns were extremely unsteady for all rotor heights tested. For a wheel height of 20 ft the flow beneath the rotor disk at ground level was shown to be towards the fuselage for the inner 2/3 of the rotor radius. Only flow outside the rotor disk at ground level was close to radial outflow.

A Navier-Stokes CFD computation for the UH-60 helicopter at 20-ft wheel height above ground was described and discussed in detail, and the computational results compared with full-scale UH-60 tuft observations (airframe and ground plane).

Results from a CFD computation for the EH-101 helicopter were described in detail and a possible explanation for the superior brownout behavior of the EH-101 suggested.

Future Work

No conclusive statements can be made as to why the EH-101 performs unusually well under brownout conditions based on the current study, but the EH-101 airframe is a reasonable suspect. A logical next step is to repeat the UH-60 computations using the

turbulent ROT3DC code and validate the results using the existing full-scale tuft data (as described for the OVERFLOW 2 code). Once the ROT3DC code has been validated, change the UH-60 airframe size, shape, and position to reflect that of the EH-101 (keeping all other variables at UH-60 levels, including C_T). Then change C_T from the UH-60 value of 0.0065 to the EH-101 value of 0.0100. These computations should then provide sufficient information to indicate whether the airframe is a dominant parameter in determining brownout severity.

Tuft images of the OH-58C, MD-500, and Yamaha RMAX still remain to be analyzed in as much detail as the UH-60L. These images will provide validation for general airframe and ground tuft pattern characteristics. In addition, since these aircraft were tufted on both sides of the airframe, the images will provide information about any flow asymmetry caused by direction of blade rotation.

Acknowledgements

The U. S. Army Aeroflightdynamics Directorate (AMRDEC) RDECOM, and the National Aeronautics and Space Administration provided funding for this project. The authors would like to recognize Dr. William Warmbrodt for his valuable insight, encouragement, and support throughout this effort. In addition, thanks go to George Tucker, Cahit Kitaplioglu, Anita Abrego, Paul Langston, Dominic Hart, and Shirley Burek for their help with the full-scale tuft tests. Thanks also go to the 2006 Aeromechanics Branch summer interns for installing the thousands of ground plane and airframe tufts. Finally, thanks go to the students at Iowa State University who helped with the EH-101 CFD calculations.

References

1. Liewer, S., "Desert Landings Rattle Pilots' Nerves," *Stars and Stripes*, April 14, 2003.
2. Sabbagh, L., "Flying Blind in Iraq: U.S. Helicopters Navigate Real Desert Storms," *Popular Mechanics*, October 3, 2006.
3. Brower, M., "Preventing Brownout," *Special Operations Technology*, Vol. 2, No. 4, July 2004.
4. Wachspress, D.A., "Advanced Rotorcraft Brownout Aerodynamic Analysis and Flight Simulation," 2nd Annual Joint Search and Rescue Conference, Georgetown University Conference Center, Washington D.C., October 1, 2007.
5. Harrison, R., Stacey, S. and Hansford, B., "BERP IV: The Design, Development and Testing of an Advanced Rotor Blade," American Helicopter Society 64th Annual Forum, Montreal, Canada, April 29-May 1, 2008.
6. Phillips, C. and Brown, R., "Eulerian Simulation of the Fluid Dynamics of Helicopter Brownout," American Helicopter Society 64th Annual Forum, Montreal, Canada, April 29-May 1, 2008.
7. Haehnel, R.B., Moulton, M.A., Wenren, Y. and Steinhoff, J., "A Model to Simulate Rotorcraft-Induced Brownout," American Helicopter Society 64th Annual Forum, Montreal, Canada, April 29-May 1, 2008.
8. Keller, J.D., Whitehouse, G.R., Wachspress, D.A., Teske, M.E. and Quackenbush, T.R., "A Physics-Based Model of Rotorcraft Brownout for Flight Simulation Applications," American Helicopter Society 62nd Annual Forum, Phoenix, AZ, May 9-11, 2006.
9. Lee, T.E., Leishman, J.G. and Ramasamy, M., "Fluid Dynamics of Interacting Blade Tip Vorticies With a Ground Plane," American Helicopter Society 64th Annual Forum, Montreal, Canada, April 29-May 1, 2008.
10. Wachspress, D.A., Keller, J.D., Quackenbush, G.R. and Yu, K., "High Fidelity Rotor Aerodynamic Module for Real-Time Rotorcraft Flight Simulation," American Helicopter Society 64th Annual Forum, Montreal, Canada, April 20--May 1, 2008.
11. Bagnold, R.A., *The Physics of Blown Sand and Desert Dunes,* Methuen; Dover, 1941.
12. Bell, T.E. and Phillips, T., "City-Swallowing Sand Dunes," NASA Office of Biological and Physical Research, December 6, 2002.
13. Nishimura, K. and Hunt, J.C.R., "Saltation and Incipient Suspension above a Flat Particle Bed Below a Turbulent Boundary Layer," Journal of Fluid Mechanics, Vol. 417, pp. 77-102, 2000.
14. Nygaard, T.A., Dimlanlig, A.C. and Meadow-croft, E.T., "Application of a Momentum Source Model to the RAH-66 Comanche FANTAIL," American Helicopter Society 4th Decennial Specialist's Conference on Aeromechanics, San Francisco, CA, January 21-23, 2004.
15. Nichols, R.H., Tramel R.W. and Buning, P.G., "Solver and Turbulence Model Upgrades to OVERFLOW 2 for Unsteady and High-Speed Applications," AIAA 25th Applied Aero-dynamics Conference, San Francisco, CA, AIAA-2006-2824, June 5-8, 2006.
16. Zori, L.A. and Rajagopalan, R.G., "Navier-Stokes Calculations of Rotor-Airframe

Interaction in Forward Flight," American Helicopter Society 48th Annual Forum, Washington D.C., June 3-5, 1992.
17. Rajagopalan, R.G. and Mathur, S.R., "Three Dimensional Analysis of a Rotor in Forward Flight," Journal of the American Helicopter Society, Vol. 38, No. 3, pp. 14-25, July 1993.
18. Poling, D.R., Rosenstein, H. and Rajagopalan, R.G., "Use of a Navier-Stokes Code in Understanding Tiltrotor Flowfields in Hover," American Helicopter Society 52nd Annual Forum, Washington D.C., June 4-6, 1996.
19. Rajagopalan, R.G. and Lim, C.K., "Laminar Flow Analysis of a Rotor in Hover," Journal of the American Helicopter Society, Vol. 36, No. 1, pp. 12-23, January 1991.

Aircraft	Disk Loading (lb/ft^2)		
	Empty Weight	**8000 lb Load**	**Maximum Weight**
CH-47D	4.7	6.3	10.0
HH-60G	5.5	9.0	10.8
EH-101	6.9	9.7	11.0
S-92	6.5	9.7	11.4
CH-53E	6.8	8.4	14.2
V-22	17.0	21.1	24.3

Table 1. Disk Loading of helicopters commonly flown in brownout conditions.

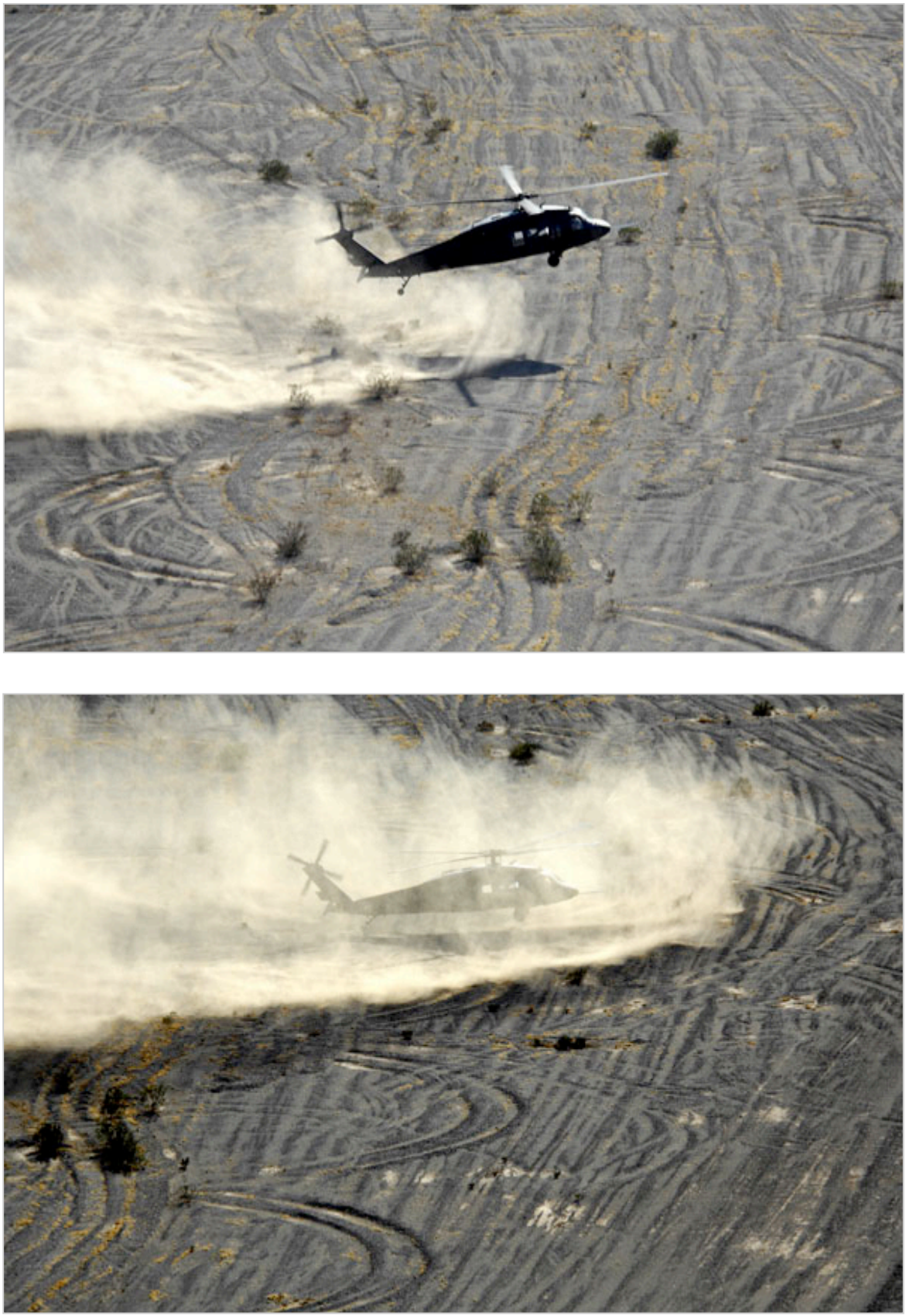

Figure 1. UH-60 Blackhawk performing test landing in brownout at Yuma Proving Grounds.

Figure 2. BERP IV blade tip design [5].

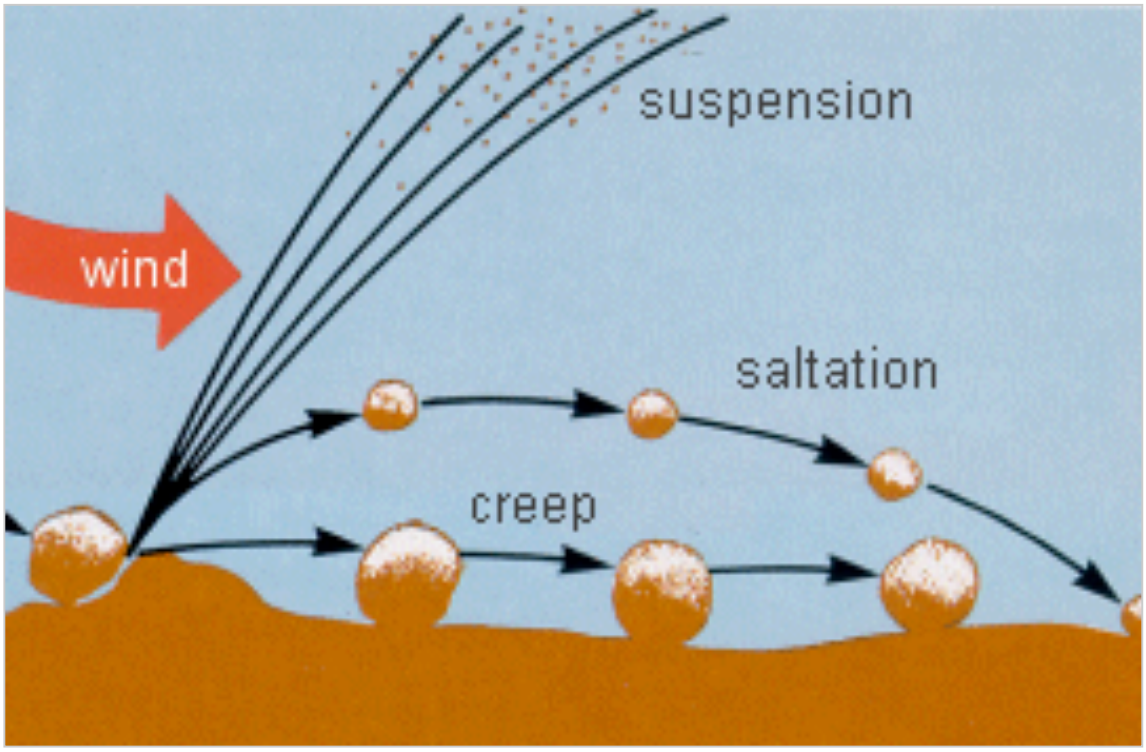

Figure 3. Particle entrainment processes [12].

Figure 4(a). Single instantaneous airframe tuft pattern; Wheel height=50 ft.

Figure 4(b). Single instantaneous airframe tuft pattern; Wheel height=50 ft.

Figure 4(c). Single instantaneous airframe tuft pattern; Wheel height=50 ft.

Figure 4(d). Overlay of three instantaneous airframe tuft images; Wheel height=50 ft.

Figure 4. UH-60 airframe tufts in hover at 50-ft wheel height (OGE).

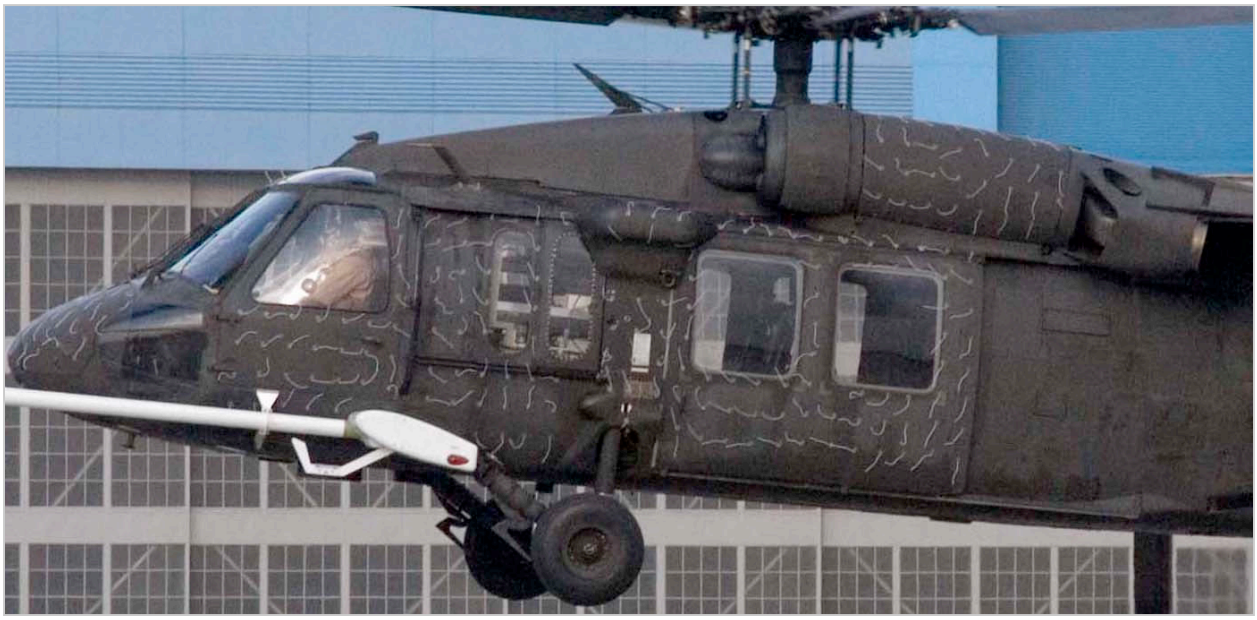

Figure 5(a). Single instantaneous airframe tuft pattern; Wheel height=5 ft.

Figure 5(b). Single instantaneous airframe tuft pattern; Wheel height=5 ft.

Figure 5(c). Single instantaneous airframe tuft pattern; Wheel height=5 ft.

Figure 5(d). Overlay of three instantaneous airframe images; Wheel height=5 ft.

Figure 5. UH-60 airframe tufts in hover at 5-ft wheel height (IGE).

Figure 6. Original UH-60 instantaneous ground plane tuft image; Wheel height=0 ft.

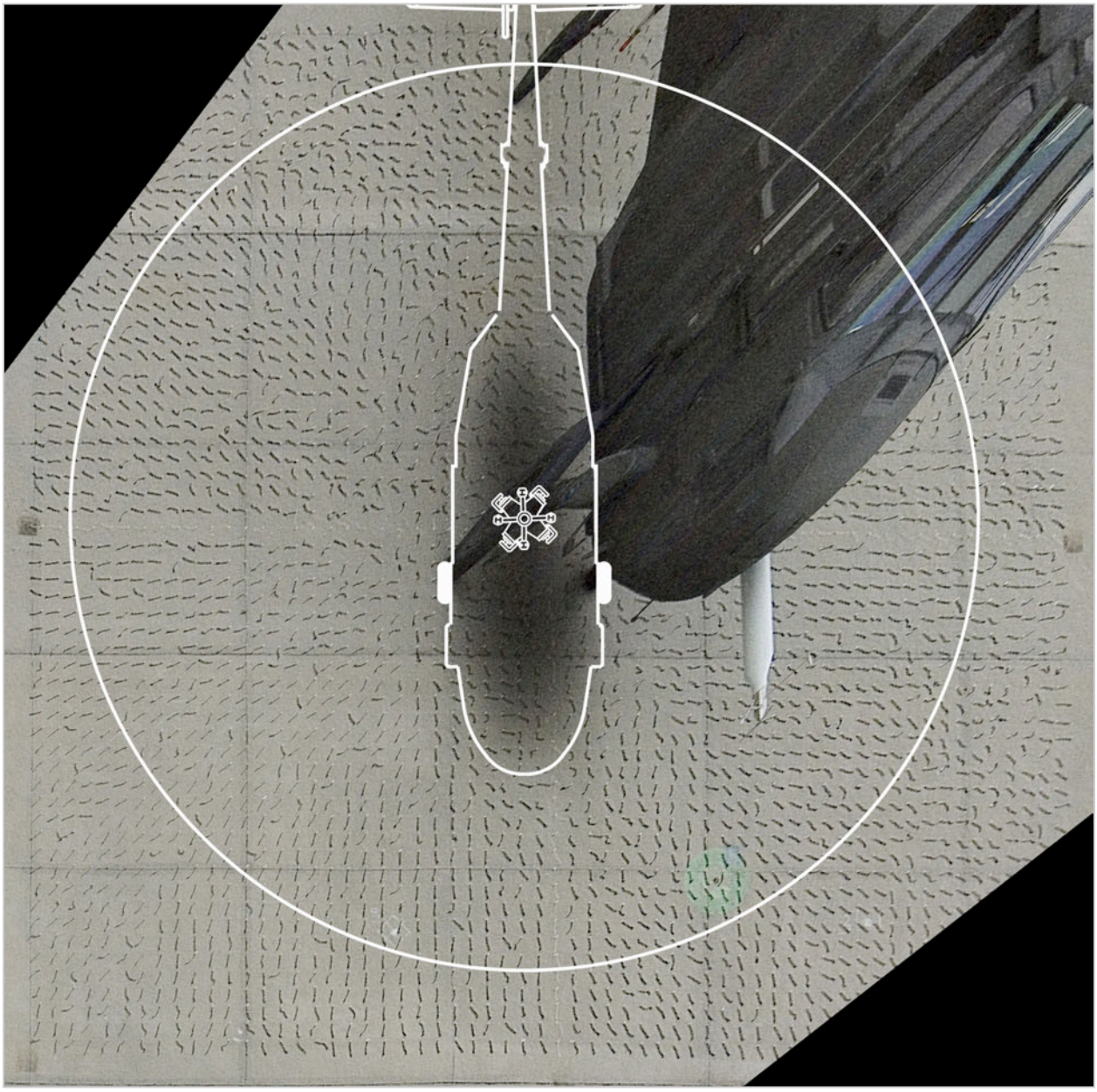

Figure 7. Reoriented UH-60 instantaneous ground plane tuft image; Wheel height=0 ft.

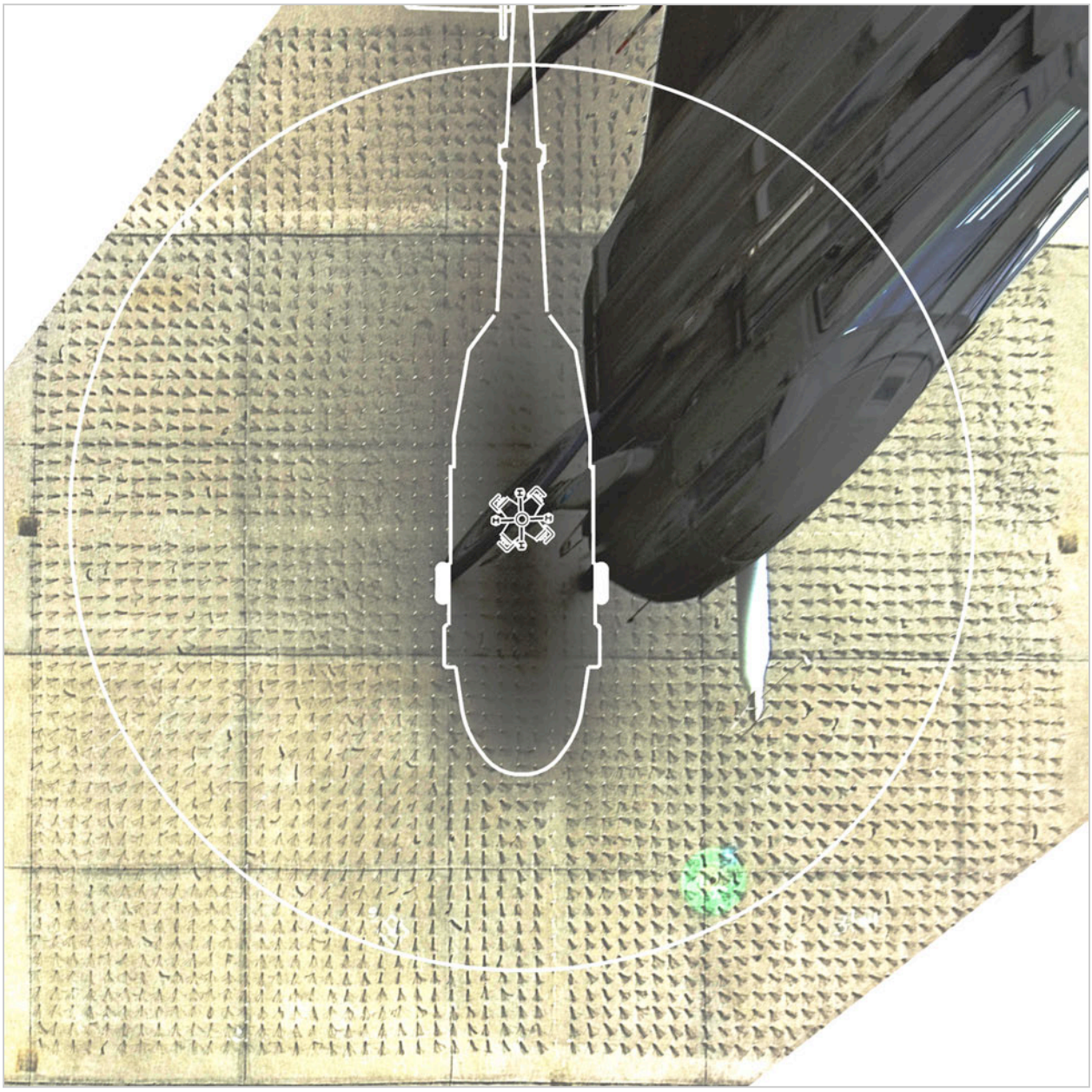

Figure 8. Reoriented average of 25 UH-60 instantaneous ground plane tuft images; Wheel height=0 ft.

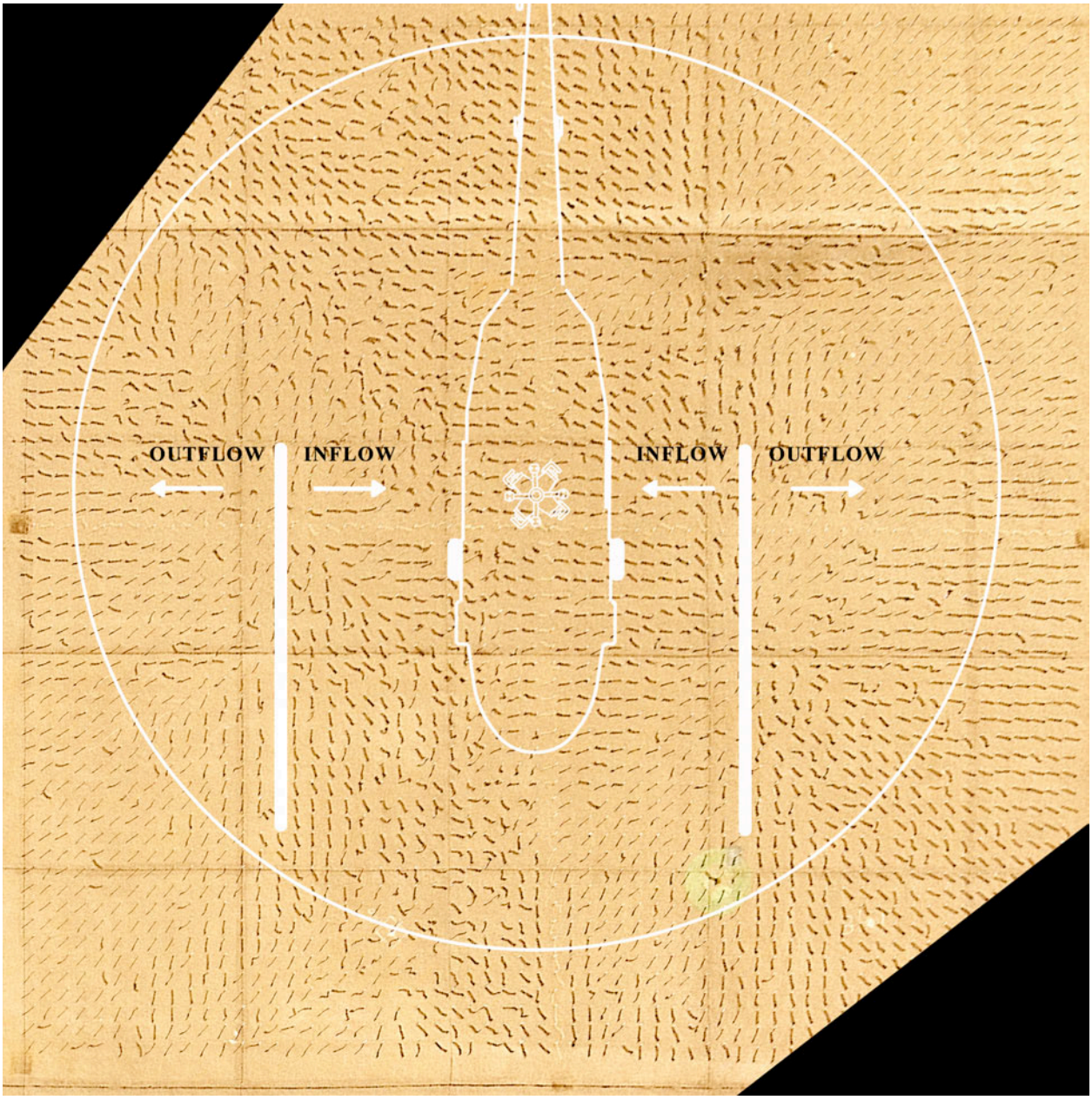

Figure 9. Reoriented UH-60 instantaneous ground plane tuft image; Wheel height=20 ft.

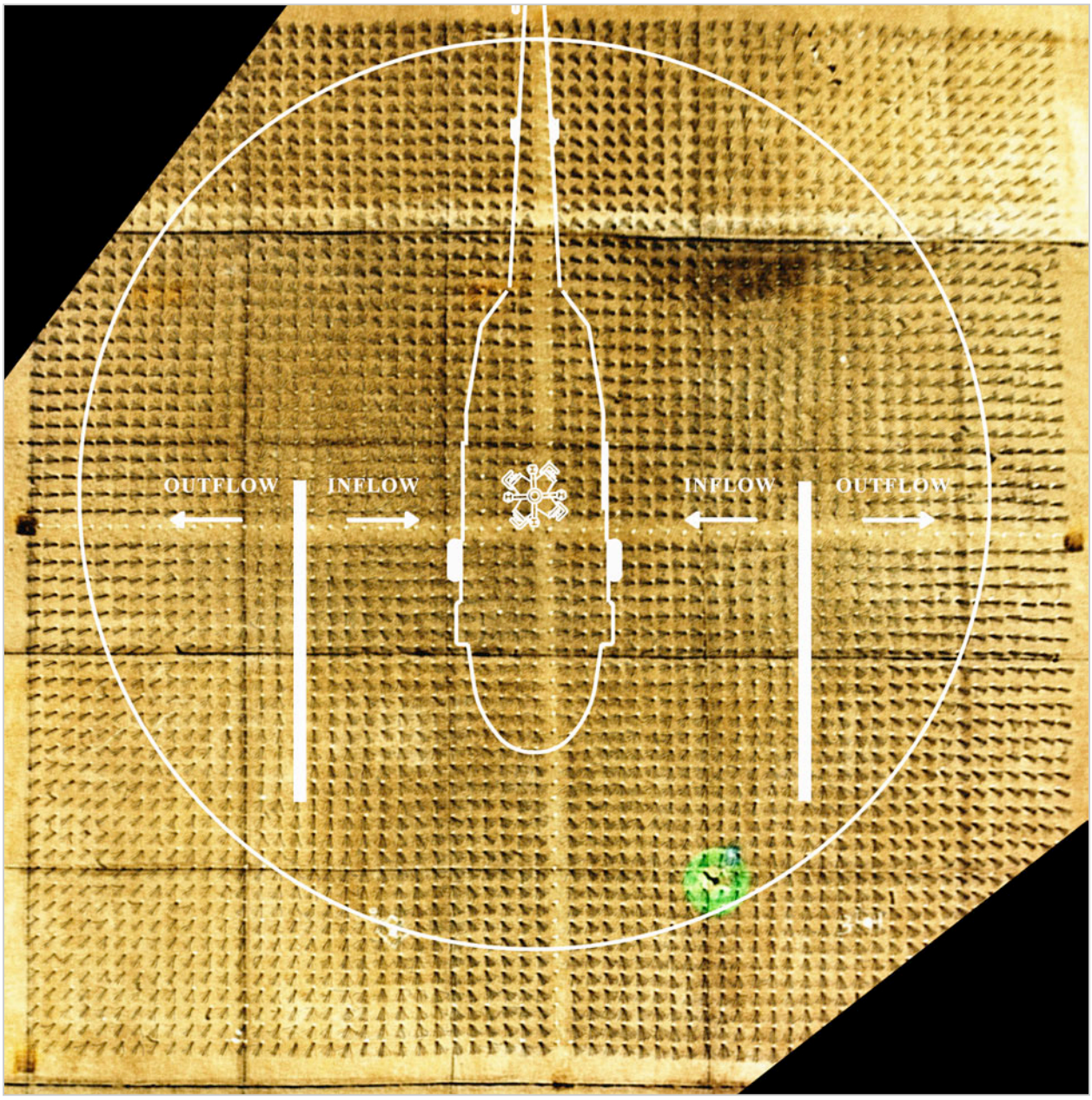

Figure 10. Reoriented average of 100 UH-60 instantaneous ground plane tuft images; Wheel height=20 ft.

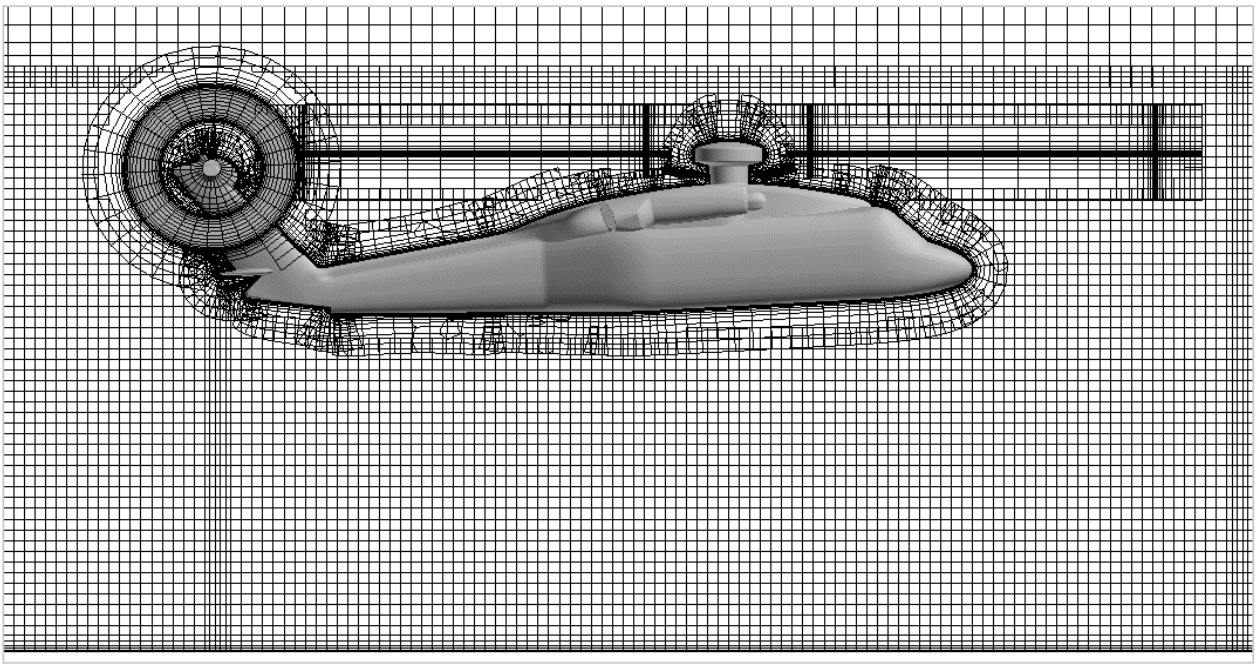

Figure 11. UH-60 CFD grid (every other point shown).

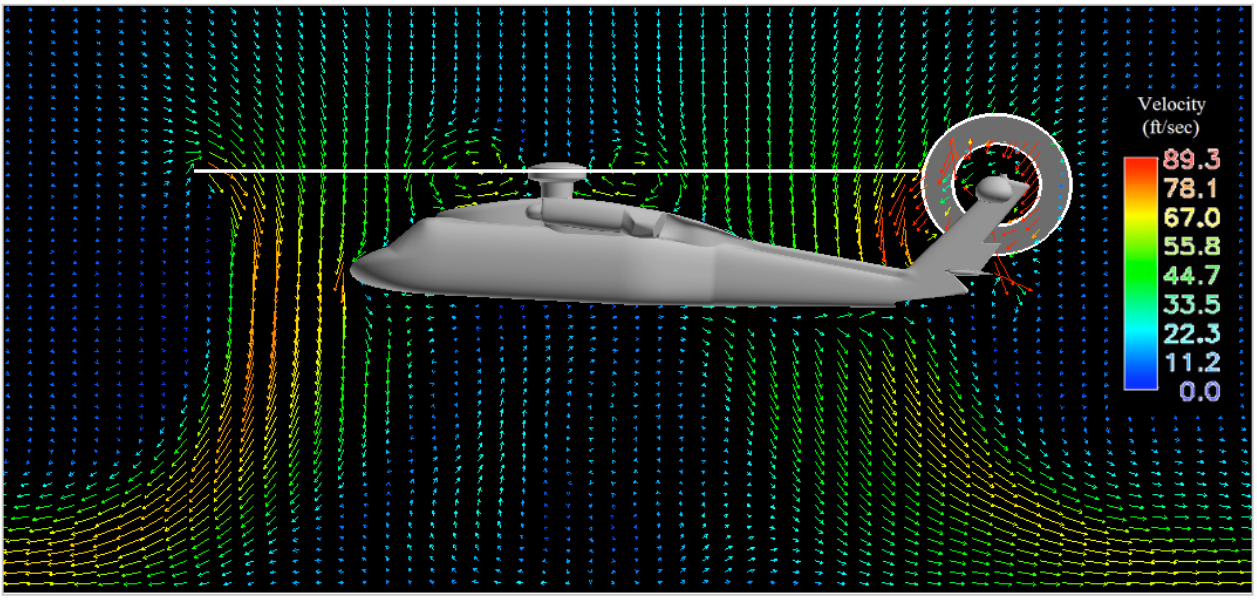

Figure 12. Mean velocity components in centerline plane for UH-60.

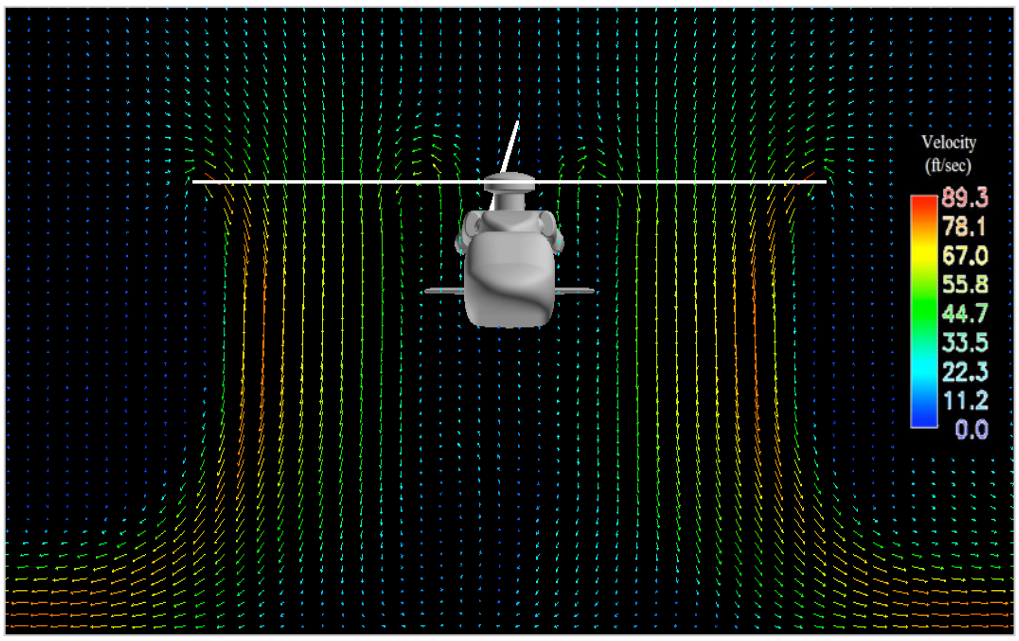

Figure 13. Mean velocity components in transverse plane through rotor hub for UH-60.

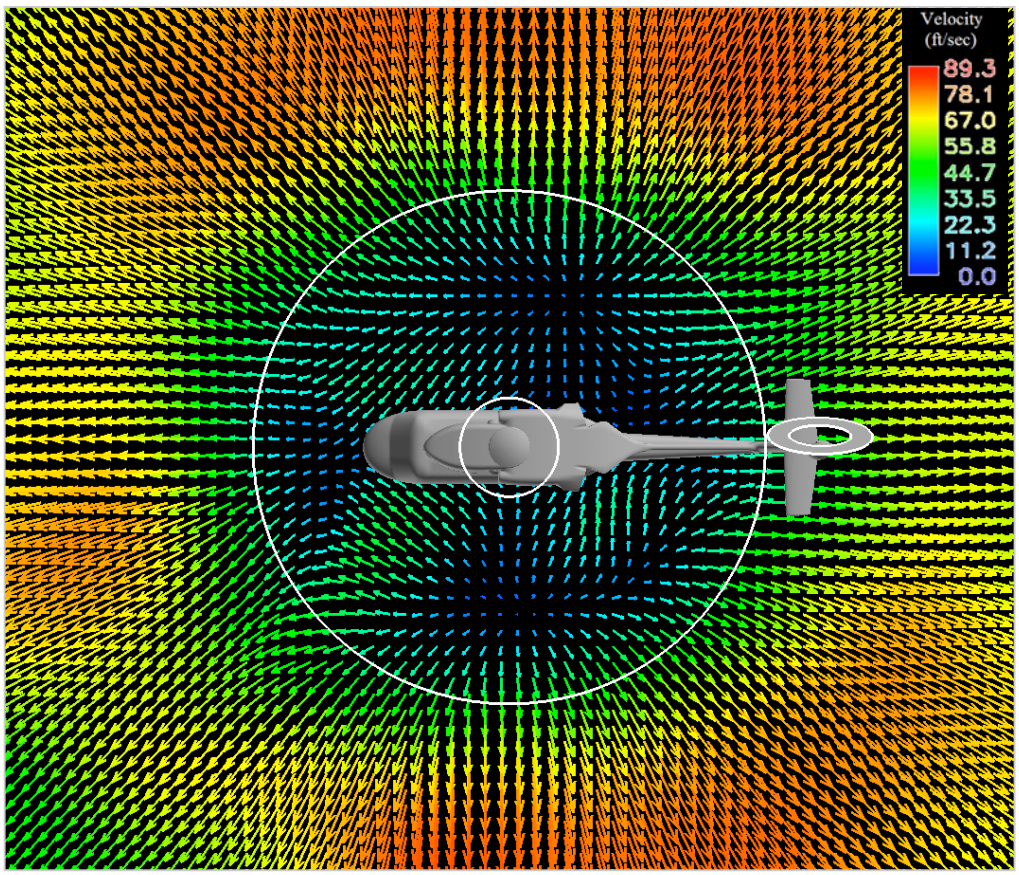

Figure 14. Mean velocity components in horizontal plane 1 ft above ground for UH-60.

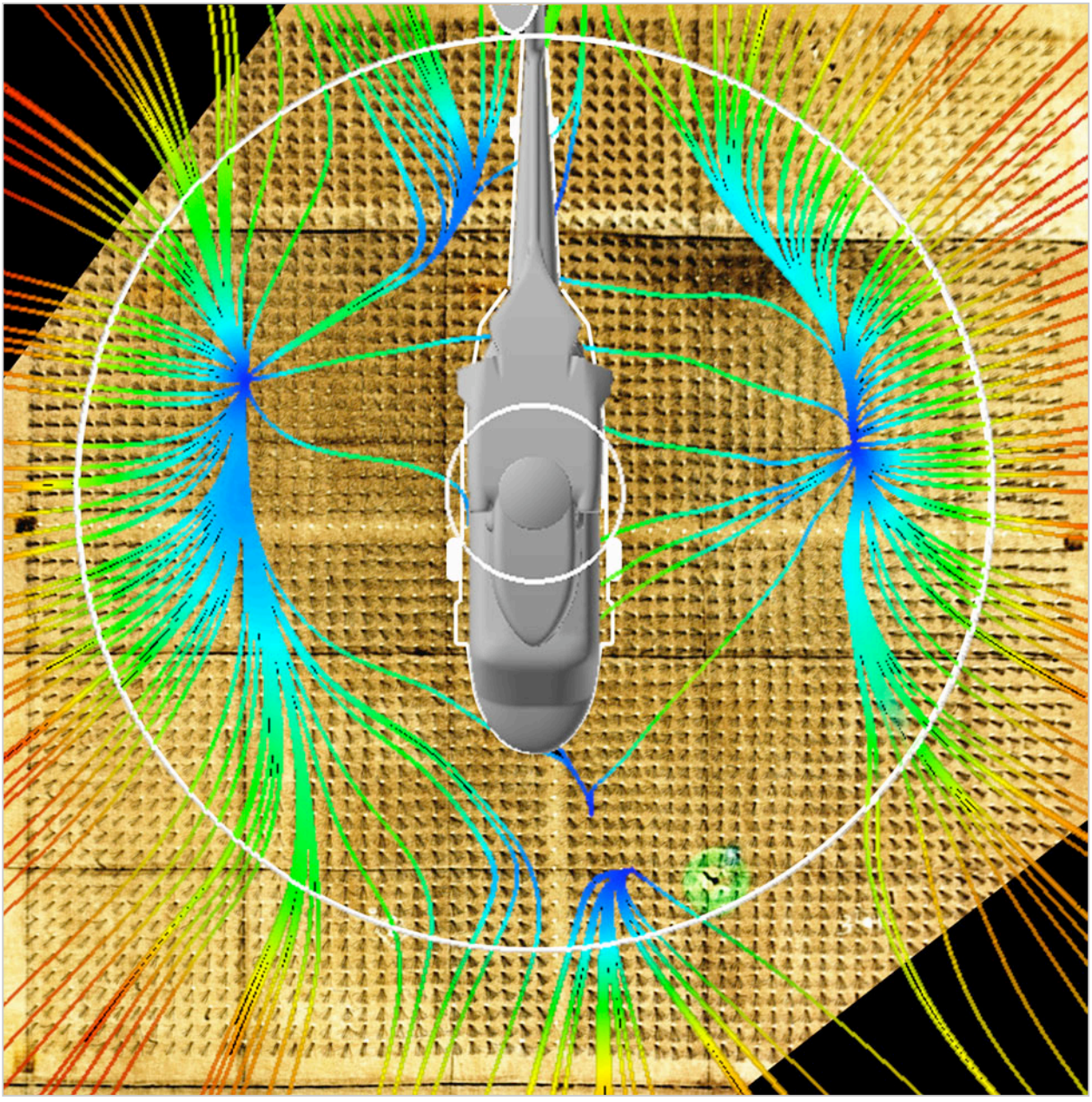

Figure 15. Overlay of computed mean surface flow lines on average ground plane tuft pattern for UH-60 (from Figure 10).

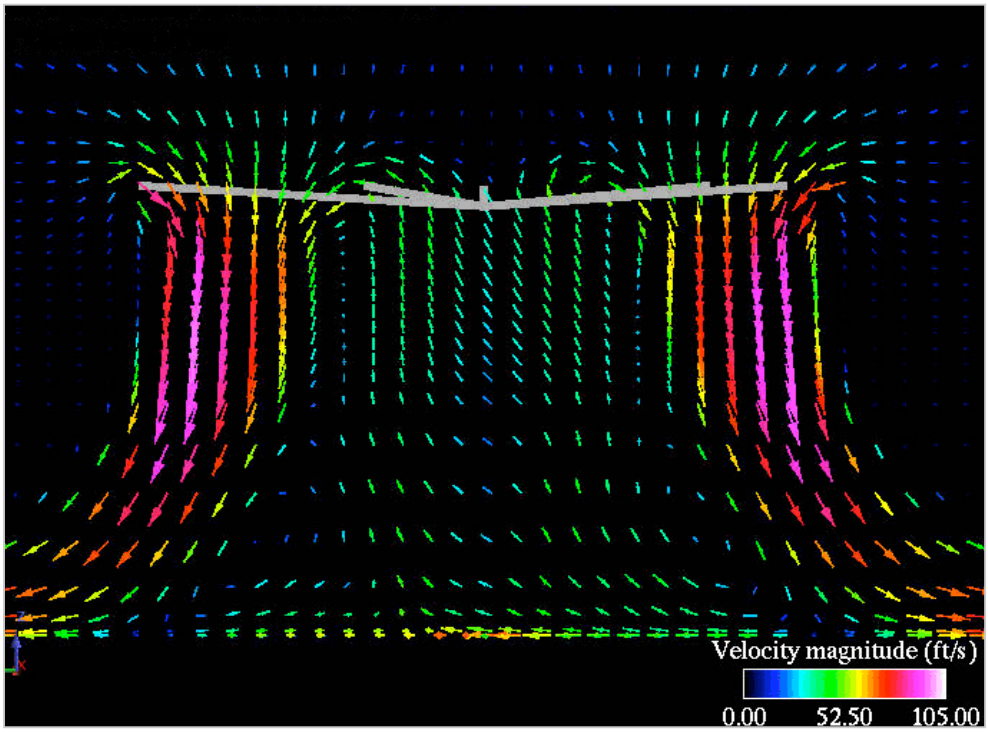

Figure 16. Velocity vectors in transverse plane for EH-101 (rotor without root cutout).

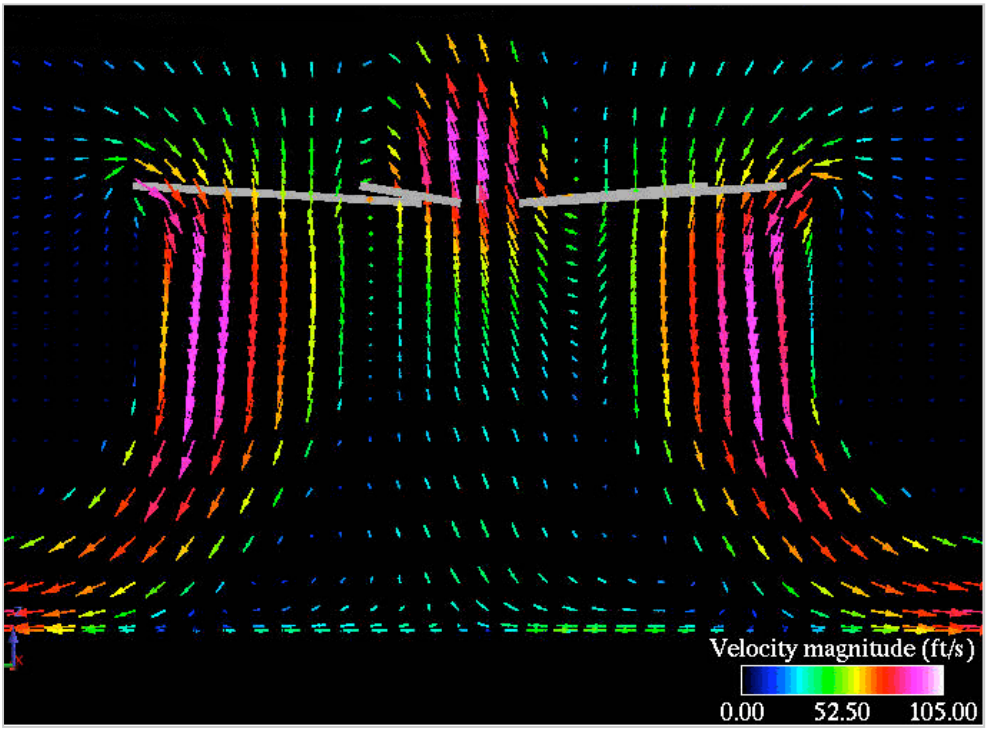

Figure 17. Velocity vectors in transverse plane for EH-101 (rotor with root cutout).

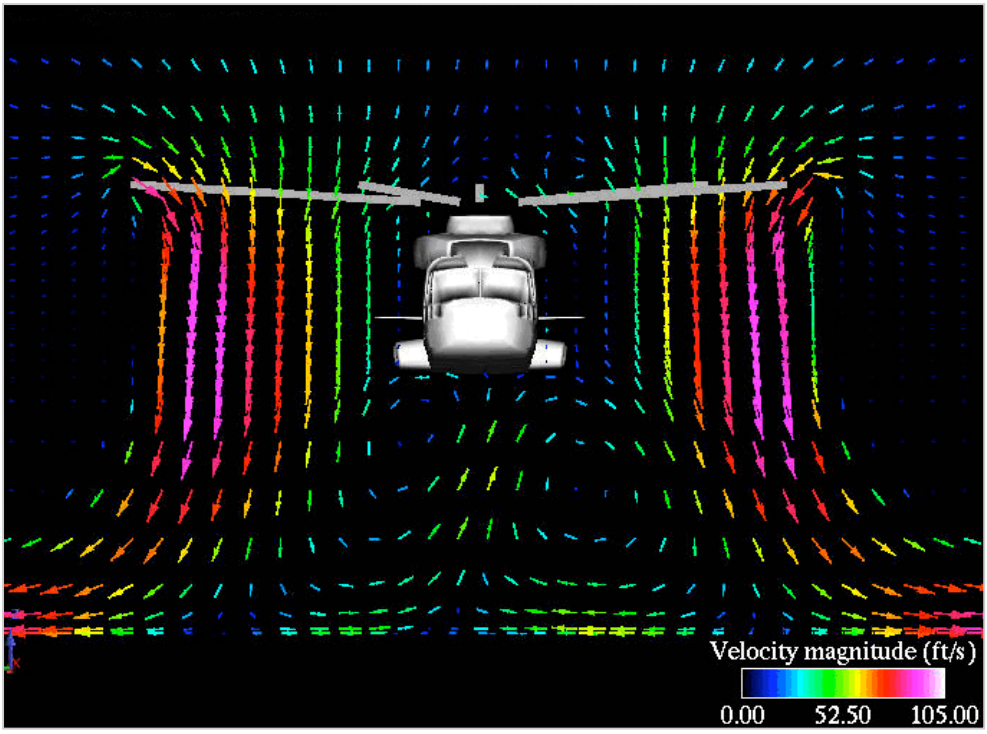

Figure 18. Velocity vectors in transverse plane for EH-101 (fuselage and rotor).

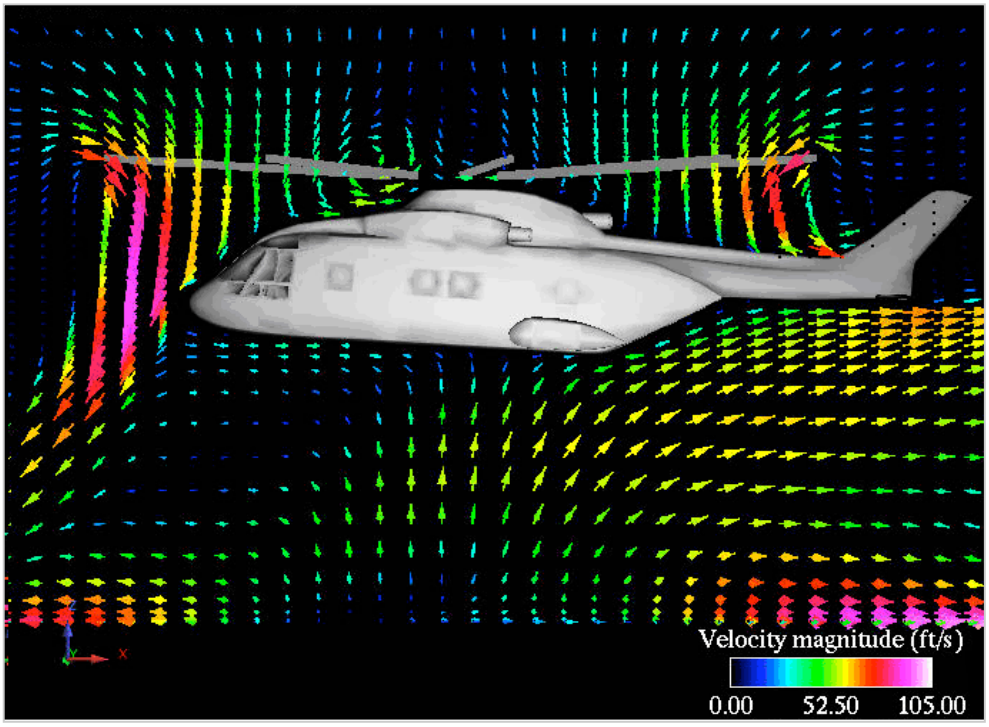

Figure 19. Velocity vectors in centerline plane for EH-101.

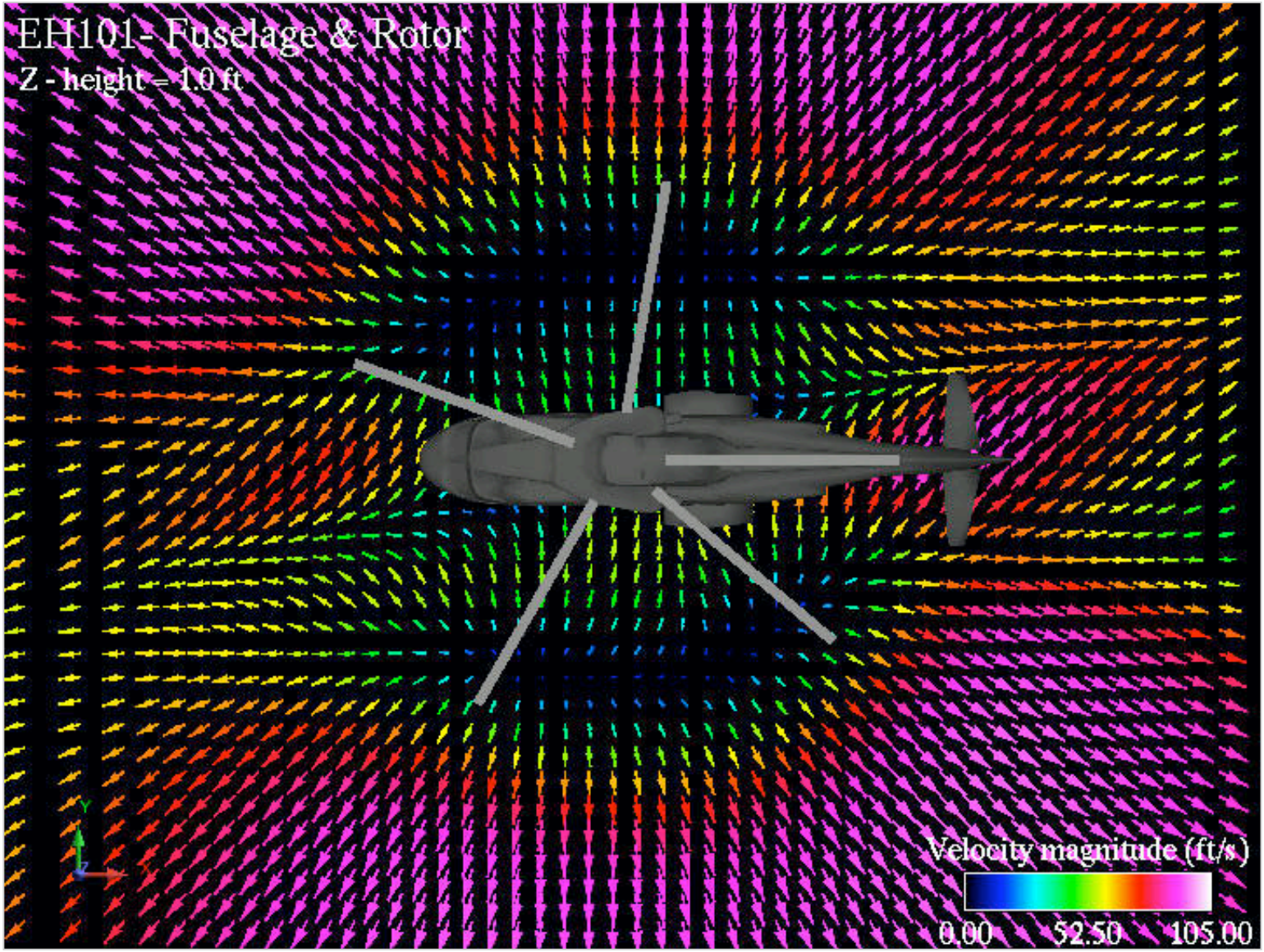

Figure 20. Velocity vectors in horizontal plane 1 ft above ground for EH-101.